Diagnosing the Sensitivity of Local Land–Atmosphere Coupling via the Soil Moisture–Boundary Layer Interaction

JOSEPH A. SANTANELLO JR. AND CHRISTA D. PETERS-LIDARD

Hydrological Sciences Branch, NASA GSFC, Greenbelt, Maryland

SUJAY V. KUMAR

Hydrological Sciences Branch, NASA GSFC, Greenbelt, Maryland, and Science Applications International Corporation, McLean, Virginia

(Manuscript received 31 October 2010, in final form 17 February 2011)

ABSTRACT

The inherent coupled nature of earth's energy and water cycles places significant importance on the proper representation and diagnosis of land–atmosphere (LA) interactions in hydrometeorological prediction models. However, the precise nature of the soil moisture–precipitation relationship at the local scale is largely determined by a series of nonlinear processes and feedbacks that are difficult to quantify. To quantify the strength of the local LA coupling (LoCo), this process chain must be considered both in full and as individual components through their relationships and sensitivities. To address this, recent modeling and diagnostic studies have been extended to 1) quantify the processes governing LoCo utilizing the thermodynamic properties of mixing diagrams, and 2) diagnose the sensitivity of coupled systems, including clouds and moist processes, to perturbations in soil moisture. This work employs NASA's Land Information System (LIS) coupled to the Weather Research and Forecasting (WRF) mesoscale model and simulations performed over the U.S. Southern Great Plains. The behavior of different planetary boundary layers (PBL) and land surface scheme couplings in LIS–WRF are examined in the context of the evolution of thermodynamic quantities that link the surface soil moisture condition to the PBL regime, clouds, and precipitation. Specifically, the tendency toward saturation in the PBL is quantified by the lifting condensation level (LCL) deficit and addressed as a function of time and space. The sensitivity of the LCL deficit to the soil moisture condition is indicative of the strength of LoCo, where both positive and negative feedbacks can be identified. Overall, this methodology can be applied to any model or observations and is a crucial step toward improved evaluation and quantification of LoCo within models, particularly given the advent of next-generation satellite measurements of PBL and land surface properties along with advances in data assimilation schemes.

1. Introduction

The inherent coupled nature of earth's energy and water cycles places significant importance on the proper representation and diagnosis of land–atmosphere (LA) interactions in hydrometeorological prediction models (Entekhabi et al. 1999; Betts and Silva Dias 2010). Unfortunately, the disparate resolutions and complexities of the governing processes have made it difficult to quantify these interactions in models or observations (Angevine 1999; Betts 2000; Cheng and Steenburgh 2005; Gu et al. 2006). For example, the impact of soil moisture on precipitation (and vice versa) is largely determined by a series of nonlinear processes ranging from soil moisture dynamics to planetary boundary layer (PBL) turbulence. As a whole, these processes determine the ''strength'' of the coupling between the land surface and atmosphere, which, as a result, varies as a function of heat and moisture fluxes that are dependent on many different LA properties, such as vegetation height, soil type, and the large-scale forcing (Jacobs and de Bruin 1992).

While it is critical to accurately represent the relationship between soil moisture (SM) and precipitation (P) and resultant LA coupling strength in models (particularly for a changing climate), a proper understanding and ultimate improvement will only come by careful examination and quantification of the full series of interactions and feedbacks (i.e., links in the chain). Recent coordinated

Corresponding author address: Joseph A. Santanello Jr., NASA GSFC Code 614.3, Bldg. 33, Room G220, Greenbelt, MD 20771.
E-mail: Joseph.A.Santanello@nasa.gov

DOI: 10.1175/JHM-D-10-05014.1

© 2011 American Meteorological Society

modeling efforts such as the Global Land-Atmosphere Coupling Experiments (GLACE; Koster et al. 2004) have been successful in identifying the relative strengths of SM–*P* coupling in various global climate models (GCMs). However, these results do not provide the process-level understanding of the mechanisms and LA parameterizations that govern the overall coupling along with the observations on the necessary scales to evaluate the accuracy of the coupling strength itself (Dirmeyer et al. 2006, 2008).

From a regional perspective, the ongoing African Monsoon Multidisciplinary Analysis (AMMA) Land Surface Model (LSM) Intercomparison Project (ALMIP; Boone et al. 2009) aims to evaluate the accuracy and formulations of offline LSMs pertaining to the SM–*P* relationship (mostly notably evapotranspiration) over a range of scales. However, as was the case for the Project for the Intercomparison of Land Surface Parameterization Schemes (PILPS; Henderson-Sellers et al. 1993) project, the results of these efforts are limited by the lack of atmospheric feedback when running in uncoupled mode.

As a result, there has been recent momentum built by studies of local LA coupling (hereafter LoCo) that attempt to take into account the full set of links in the SM–*P* process chain. By exploiting the role of the convective PBL as a short-term memory of land surface processes (through the integration of regional surface fluxes on diurnal scales), the balance of fluxes and states established between the land surface and mixed layer can be used as a diagnostic of the degree of coupling and the impact of feedbacks within the LA system (Pan and Mahrt 1987; Oke 1987; Diak 1990; Dolman et al. 1997; Peters-Lidard and Davis 2000; Cleugh et al. 2004; Betts and Viterbo 2005; Santanello et al. 2005, 2007). To this end, significant progress has been made in identifying individual LA processes and feedback loops for a particular location or model (Sorbjan 1995; Eltahir 1998; Margulis and Entekhabi 2001; Barros and Hwu 2002; Steeneveld et al. 2006).

A comprehensive approach to diagnose the full nature of LoCo has recently been developed that can be applied to any model and evaluated against observations (Santanello et al. 2009; hereafter S09). Based on the mixing diagram theory of Betts (1992), this approach offers the ability to perform a robust evaluation of LA interactions using routinely available inputs due to the integrative nature of the PBL on diurnal time scales. S09 demonstrated this methodology using a coupled, high-resolution, mesoscale model with multiple LSMs and PBL schemes (PBLs), thereby showing the variation in LA coupling among different scheme combinations for a series of daily simulations. The true utility of this work, however, comes in enabling the governing processes (i.e., fluxes) and links in the chain (i.e., feedbacks) to be quantified in such models and ultimately evaluated against observations to diagnose the overall nature and accuracy of LoCo in each.

With these issues in mind, this paper extends the work of S09 in order to: 1) quantify the processes governing local LA coupling utilizing the thermodynamic properties of mixing diagrams, and 2) diagnose the sensitivity of coupled systems, including clouds and moist processes, to perturbations in soil moisture. Rather than performing a rigorous model evaluation or intercomparison against observations, the focus is on developing the framework for identifying LoCo processes and incorporating this methodology into the modeled results of S09 and new experiments described here. Section 2 of this paper presents an overview of recent progress in LoCo research and summarizes the results of S09 that are adopted and extended in this study. The coupled mesoscale model, land surface models, and PBLs used in the experiments are described in section 3 along with detailed information on the sites, experimental period, and associated observations. Results and analyses applied to these experiments are presented in section 4. Finally, a summary and discussion of the greater applicability of these results in the context of current and future LoCo research is given in section 5.

2. Background

A thorough review of LoCo research efforts and motivation can be found in S09. Here, we focus more closely on recent studies that have been converging in their understanding and treatment of LA interactions. It is therefore useful to describe exactly what is meant by local rather than nonlocal (or global–large-scale) coupling. The realm of LoCo has been defined most recently by the Global Land/Atmosphere System Study (GLASS; www.gewex.org/glass.html) as the following: ''The temporal and spatial scale of all land-surface related processes that have a direct influence on the state of the PBL'' (Van den Hurk and Blyth 2008, p. 13). The fundamental processes that fall into this realm include the direct moistening–drying and heating–cooling of the PBL and the feedback exerted by this PBL change on the surface fluxes (through PBL growth and entrainment), the subsequent formation–disappearance of PBL clouds and triggering–fueling of convection, and the accumulation of hydrological anomalies in the soil reservoir and their subsequent impacts on the energy balance (Van den Hurk and Blyth 2008). Inherent in this definition is the importance of the diurnal interaction (e.g., convective PBL evolution) in contrast to the seasonal and long-term perspective of GLACE.

From a LoCo perspective, the SM–*P* relationship can be broken down into two main components:

$$\frac{d(P)}{d(\mathrm{SM})} = \frac{d(\mathrm{EF})}{d(\mathrm{SM})} \times \frac{d(P)}{d(\mathrm{EF})}, \tag{1}$$

where EF is the evaporative fraction, defined as

$$\mathrm{EF} = \frac{LE_{\mathrm{sfc}}}{H_{\mathrm{sfc}} + LE_{\mathrm{sfc}}}. \tag{2}$$

The quantity EF is a function of the sensible (H_{sfc}) and latent (LE_{sfc}) heat fluxes at the land surface and ranges from 0 to 1 for dry and freely evaporating surfaces, respectively. Based on these formulations, there have been numerous studies focusing on the relationship between SM and EF at the land surface, and a distinct branch of research focused on larger scale EF–P or SM–P interactions that are typically outside the realm of LoCo (Seneviratne et al. 2010).

a. Soil moisture–evaporation relationship

The SM–EF link has been well-explored, particularly in the context of the surface (canopy) layer coupling. Jarvis and McNaughton (1986) explicitly derived a decoupling factor Ω that quantifies how tightly surface conditions and those at screen level (reference height) are coupled. The decoupling factor ranges from 0 to 1, and is formally a function of the ratio of surface (rs) to aerodynamic (canopy; ra) resistance. As a result, forested surfaces (high rs, low ra) are considered strongly coupled while smooth grasslands (low rs, high ra) are weakly coupled. As suggested by Monteith and Unsworth (1990) and Jacobs and de Bruin (1992), however, the term "coupling" in this work is not entirely representative of LoCo because of the absence of PBL feedback. In fact, Jacobs and de Bruin (1992) have shown that the sensitivity of EF to rs and ra is dependent on the magnitude and sign of PBL feedback, which must be included when evaluating coupled models.

While Ω is limited to identifying when surface- versus reference-level conditions are important in determining EF, the full sensitivity of the SM–EF relationship has recently been derived by Jacobs et al. (2008). This was done by linking the sensitivity of rs to SM (using typical LSM formulations) with that of EF to rs (from Jacobs and de Bruin 1992), and through the Penman–Monteith equation is related back to the decoupling factor as follows:

$$\frac{d(\mathrm{EF})}{d(\mathrm{SM})} = \frac{\mathrm{EF}}{\mathrm{SM} - \mathrm{SM}_{\mathrm{wilt}}} \times (1 - \Omega), \tag{3}$$

where $\mathrm{SM}_{\mathrm{wilt}}$ is the wilting point of the soil. This formulation is important because it describes exactly how surface heat and moisture fluxes are impacted by a change in SM, and incorporates the local (soil and vegetation) conditions. Once again, it is useful only from an offline LSM (or land data assimilation) perspective when isolating the SM–EF relationship, and does not capture the modulation from PBL feedbacks on the system.

In a similar vein, Chen and Zhang (2009) have isolated the impact of surface exchange coefficients on LoCo. These coefficients of heat (Ch) and moisture (Cm) determine, in part, the efficiency of transporting heat and moisture from the surface to the overlying atmosphere such that their magnitudes are proportional to sensible and latent heat fluxes, respectively. By backing out Ch and Cm from long-term observations of screen-level variables and fluxes, their values over different land cover conditions were then compared with those typically employed in LSMs. While also useful from an offline LSM evaluation and development perspective, this work in isolation, and in particular the equating of coupling strength with the magnitude of Ch alone is miscast. For example, Ch here is directly mapped to land cover and treated as the sole determinant of coupling strength without regard for the atmospheric regime or PBL feedback.

b. Evaporation–precipitation relationship

As shown in the previous section, a comprehensive diagnosis of LoCo requires the additional links in the process chain beyond SM–EF, which represents the PBL feedback. The full set of LA processes to be considered can therefore be summarized as follows:

$$\Delta\mathrm{SM} \underset{(a)}{\rightarrow} \Delta\mathrm{EF}_{\mathrm{sm}} \underset{(b)}{\rightarrow} \Delta\mathrm{PBL} \underset{(c)}{\rightarrow} \Delta\mathrm{ENT} \underset{(d)}{\rightarrow} \Delta\mathrm{EF}_{\mathrm{atm}} \blacktriangleright \Delta P/\mathrm{Clouds}. \tag{4}$$

The impact of soil moisture (ΔSM) on clouds and precipitation (ΔP) is therefore dependent on the sensitivities of the following: (a) the surface fluxes ($\mathrm{EF}_{\mathrm{sm}}$) to soil moisture, (b) PBL evolution to surface fluxes, (c) entrainment fluxes at the PBL top (ENT) to PBL evolution, and (d) the collective feedback of the atmosphere (through the PBL) on surface fluxes ($\mathrm{EF}_{\mathrm{atm}}$). As a result, there are numerous pathways composed of positive and negative feedback loops inherent in this chain, which have been detailed by Santanello et al. (2007) and Van Heerwaarden et al. (2009). In particular, interaction (d) is typically not addressed in offline or surface–vegetation layer modeling studies, and represents the connection of changes at the surface to those in the PBL and free atmosphere due to entrainment.

In an effort to understand this complex set of dependent relationships, specific components of the sensitivities in Eq. (4) have been examined using coupled 1D column models. For example, the sensitivity of PBL growth was

found to be principally a function of the soil moisture regime and the initial atmospheric stability on a given day, and that soil type and vegetation amount were confounding factors limiting the direct relationship between SM and PBL height (Santanello et al. 2005, 2007). Likewise, complex and nonlinear relationships were found between EF, mixed-layer potential temperature, PBL height, and the gradient of humidity at the PBL top that drives entrainment (Δq_{ent}; Van Heerwaarden et al. 2009). These studies agree that observable properties of the system exist, but it remains difficult to gain a full understanding (or metric of quantifying) the relationships and feedbacks contained in Eq. (4).

A more formal approach to quantifying the SM–*P* relationship has been developed by Ek and Holtslag (2004) in the form of a relative humidity tendency (RH-tend) formulation applied at the top of the PBL. The RH-tend includes both evaporative (EF) and nonevaporative terms (PBL heating, growth, and entrainment), and in turn encompass the full set of EF–*P* interactions in Eq. (4). Also employing a single column model, the sensitivities to a full range of EF and PBL conditions were examined in an effort to understand the complex behavior and feedbacks that control the rise and fall of humidity (i.e., the likelihood of clouds) at the PBL top.

A significant finding was that of a positive impact of EF on RH-tend for certain LA conditions (e.g., wet soils increasing RH), but not for others (e.g., dry soils increasing RH because of entrainment effects). A similar negative feedback effect was found in a modeling study by Siqueira et al. (2009), where dry soils favored convective initiation because PBL growth was deep enough to bring in air from a rather moist free atmosphere through entrainment. Once again, the full set of LA interactions (including those of negative feedbacks) is shown to be critical to understanding the SM–*P* relationship, but depends on many factors that remain difficult to quantify.

Along these lines, De Ridder (1997) derived an analytical expression describing the relationship of equivalent potential temperature (θ_e) to EF. As defined in section 2d, θ_e is typically used as a measure of the potential for moist convection, and as such this formulation links the sensitivity of PBL evolution to the surface evaporation (EF–PBL) with the potential for *P*. The specific nature of this relationship remains strongly dependent on many assumptions regarding PBL growth (Δq_{ent}), but does provide direct insight into one critical link in the LoCo process chain.

c. *Diagnostics of LoCo: Mixing diagrams*

Recently, a methodology directly addressing the full components of Eq. (4) was outlined and tested by S09 that uses the idea of mixing diagrams as introduced by Betts (1992). This approach relates the daytime evolution of 2-m potential temperature (θ) and humidity (q) to the LA exchange of heat and moisture and the growth of the PBL. In effect, the variability of θ and q is sensitive to and integrative of the dominant processes involved in LoCo, the calculation of which requires only variables that are routinely measured and output from coupled models. For a full description of this approach and its implementation in this context the reader is referred to S09.

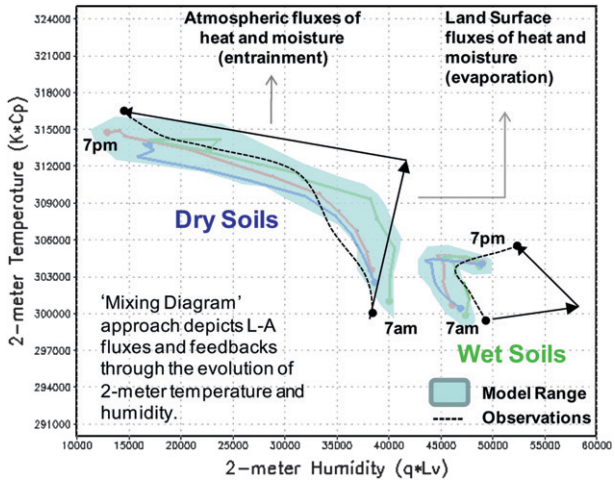

FIG. 1. Mixing diagram showing the diurnal coevolution (0700–1900 UTC) of 2-m specific humidity and 2-m potential temperature on 12 Jun 2002 at a dry and wet soil location as simulated by a coupled mesoscale model (derived from Figs. 2–5 in S09). The shaded regions for each indicate the model range for different LSM–PBL scheme couplings (red, green, and blue) vs observed (dashed black). Also shown for the dry site are the vectors that represent the fluxes of heat and moisture from the land surface vs those from the atmosphere due to entrainment, both of which are quantified using this approach.

A composite of mixing diagram results from S09 is shown in Fig. 1. Here, the coevolution of θ and q (in energy space) as simulated by a coupled mesoscale model is shown for dry and wet soil moisture locations. Simulations were run using a fully coupled modeling system, each with a different LSM–PBL scheme combination. This allows for the model to evolve in response to the LA interactions generated by each LSM–PBL combination and evaluated in relation to what was observed at each site. Overall, the results show that soil moisture anomalies (dry versus wet) lead to different patterns of θ and q evolution throughout the day. Significant warming and drying occurs at the dry site as a result of strong surface heating that leads to large PBL growth (and warm, dry air mixing in at the PBL top through entrainment). The converse is evident at the wet site, with a signature of moistening and very little warming as a result of strong surface evaporation and limited PBL growth and entrainment.

More importantly from a LoCo perspective, the evolution of θ and q can be broken down into vector components that represent the contribution of heat and moisture from the land surface versus that from the top of the PBL via entrainment. Mixing diagrams such as these therefore integrate the full nature of the LA interaction, including quantification of the governing processes (i.e., fluxes of heat and moisture). Furthermore, the spread in the model results due to different LSM–PBL combinations can then be evaluated against observations and used to pinpoint the weaknesses in either the land and/or atmospheric component of the model.

S09 also demonstrated how metrics such as the surface and entrainment Bowen ratio (β_{sfc}, β_{ent}), and the entrainment ratio of heat and moisture (A_h, A_{le}) are useful diagnostics of the LSM–PBL coupling that can be easily derived from mixing diagrams. Further, all the components of heat and moisture budgets in the PBL are derived in terms of surface, entrainment, and advection fluxes. This represents a significant extension of studies such as PILPS in that different model couplings can be intercompared and evaluated against observations in terms of their component fluxes, including those comprising the PBL feedback. Overall, this approach provides a pathway to study both the individual and collective factors determining LoCo [Eq. (4)], and most importantly can be applied equally to any model and location of interest.

d. Diagnostics of LoCo: Thermodynamic overlays

Mixing diagrams are plotted in energy space (Lq versus $C_p\theta$; where L is the latent heat of vaporization and C_p is the specific heat), which enables the vector fluxes to be derived directly (in W m^{-2}) from the evolution of θ and q. Also, considering heat and moisture simultaneously allows thermodynamic properties of the system to be overlain and thus quantified using the diagrams (Betts and Ball 1995; Betts et al. 1996). These include the following:

Relative humidity:
$$\mathrm{RH} = \frac{q}{q_s}; \tag{5}$$

Equivalent potential temperature:
$$\theta_e = \left(T + \frac{L}{c_p}r\right)\left(\frac{p_0}{p}\right)^{R_d/C_p}; \tag{6}$$

Pressure of the lifting condensation level:
$$P_{\mathrm{lcl}} = \frac{1}{\left(\frac{T - \mathrm{Td}}{223.15}\right) + 1}p_0; \quad \text{and} \tag{7}$$

Potential saturation humidity deficit:
$$\Delta q^* = q_s(\theta) - q, \tag{8}$$

where q_s is the saturation specific humidity at θ, r is the mixing ratio, p_0 is the standard (surface) reference pressure, R_d is the gas constant for air, and Td is the dewpoint temperature. This set of diagnostics effectively relates the near-surface moisture condition (as a function of EF and resulting feedback of the PBL) to that of the potential for clouds and precipitation. For example, the impact of a change in soil moisture (ΔSM) can be evaluated using mixing diagram overlays based on the corresponding changes in EF, θ and q, θ_e, P_{lcl}, PBL feedback (entrainment), Δq^*, and ultimately cloud formation (e.g., when PBL height reaches P_{lcl}).

Along these lines, studies of the concept of equilibrium evaporation have been performed by Betts and Ball (1994), Culf (1994), and Raupach (2000) that directly relate to LoCo processes and feedbacks. They have shown that under certain conditions, the LA system evolves to a state where the surface evaporation reaches equilibrium with the PBL feedback described above. In effect, this would be the analytical solution for the final sensitivity of $\Delta\mathrm{EF}_{\mathrm{atm}}$ in Eq. (4). On the time scales of interest for LoCo, this only occurs within a single diurnal cycle during very wet surface conditions, and as a result cannot typically be solved formally. However, using mixing diagrams and overlays of Δq^* (as described by Culf 1994) the tendency toward or away from an equilibrium condition and constant saturation deficit is a valuable diagnostic that can be evaluated in the context of its sensitivity to ΔSM and the LoCo process chain. Thermodynamic overlays and the equilibrium concept will be presented in section 4 as an extension of the experiments and results of S09.

3. Model and site description

a. LIS–WRF system

The Advanced Research version of the Weather Research and Forecasting Model (WRF-ARW; Michalakes et al. 2001) is a state-of-the-art mesoscale numerical weather prediction system. As described by S09, WRF-ARW has been coupled to National Aeronautics and Space Administration (NASA's) Land Information System (LIS; Kumar et al. 2006; Peters-Lidard et al. 2007) to serve as a fully interactive system for studying LA interactions (hereafter LIS–WRF). LIS consists of a suite of LSMs and provides a flexible and high-resolution representation of land surface physics and states which are directly coupled to the atmosphere. The advantages of LIS–WRF over the default WRF-ARW include the ability to spin up land surface conditions on a common

grid from which to initialize the regional model, consistency in land surface physics used in the initialization and forecast, flexible and high-resolution soil and vegetation representation, additional choices of LSMs of varying complexity and design, and features such as land data assimilation, parameter and uncertainty estimation, and ensemble simulation.

LIS–WRF has been tested extensively thus far over the U.S. Southern Great Plains (SGP), Florida, Europe, the Gulf of Mexico, and Korea. The experiments conducted by S09 employed LIS version 5.0 coupled to WRF-ARW version 2.2 (Kumar et al. 2008). For the sake of consistency, the extension of the results of S09 presented in section 4a are based on simulations using same version of the LIS–WRF code as was used in that study.

1) LAND SURFACE MODELS

The LSMs employed in LIS for this study are the Noah LSM version 2.7.1 (Noah; Ek et al. 2003) and the Community Land Model version 2.0 (CLM; Dai et al. 2003). Each model dynamically predicts water and energy fluxes and states at the land surface, but vary in specific parameterizations and representation of soil and vegetation properties and physics. For example, Noah solves moisture and heat transport through four discrete soil layers while CLM solves for ten layers. In addition, treatment of vegetation types and properties (such as height, coverage, and density) and canopy fluxes differ between the LSMs. Noah is used operationally by the National Centers for Environmental Prediction as the LSM for the North American Mesoscale (NAM) model and the Global Forecasting System (GFS). The CLM coupling is unique to LIS–WRF, and it should be noted that CLM serves as the LSM for NCAR's coupled Community Climate System Model (CCSM). As a result, these LSMs are well-supported and developed, and capture a wide range in complexity (layering and vegetation physics) and application (mesoscale to global climate model) of schemes evaluated during the PILPS experiments.

2) PBL SCHEMES

In WRF-ARW version 2.2, there are three options for PBL parameterizations that are rather robust and well-tested. The simplest of the three is the Medium-Range Forecast (MRF; Hong and Pan 1996) scheme, which is based on nonlocal K theory (Troen and Mahrt 1986) mixing in the convective PBL and where the diffusion and depth of the PBL are a function of the Richardson number (Ri_{cr}). The Yonsei University (YSU; Hong et al. 2006) scheme is based on the MRF and the nonlocal K theory implementation, but includes explicit treatment of entrainment and counter gradient fluxes. Finally, the Mellor–Yamada–Janjic (MYJ; Janjic 2001) scheme is the most complex of the three, and employs nonsingular level 2.5 turbulent kinetic energy (TKE) closure (from Mellor and Yamada 1982) with local K vertical mixing. In the MYJ scheme, the length scale is a function of TKE, buoyancy, and shear, and the PBL height is diagnosed based on TKE production. Overall, these three PBL schemes span the range in complexity (first order to TKE) and application (single column to full 3D) of those participating in the Global Energy and Water Cycle Experiment (GEWEX) Atmospheric Boundary Layer Study (GABLS; more information available online at www.gewex.org/gabls.htm). We therefore expect the results to encapsulate much of the range of LA coupling possible between LSMs and PBLs participating in PILPS and GABLS.

b. *Experimental design: Model and case studies*

To address LoCo under the LIS–WRF framework, simulations were performed across the array of LSMs and PBLs described above, with each enabling a different LSM–PBL combination for a total of 6 (2×3) representations of LA coupling (the remainder of the LIS–WRF setup is identical for each). The results of each simulation are then evaluated using the LoCo diagnostic approaches of S09 and described in section 2, where the processes and feedbacks generated by each LSM–PBL pair are quantified over the course of the day for different locations and conditions and compared with observations.

As shown by Koster et al. (2004) and others, the SGP region has been identified as a hotspot for LA coupling in terms of the strength of interactions and feedbacks and its role as a transitional zone of soil moisture and vegetation conditions. Because of this, and the large record of observational data in this region, S09 focused on experiments conducted for two "golden days" (6 and 12 June) during International H_2O Project in June 2002 (IHOP-02; Weckworth et al. 2004), and evaluated using data from the Atmospheric and Radiation Measurement test bed located in the region (ARM-SGP). Here, we focus on the 12 June case that was characterized by both clear sky and convectively active regions. Further details of the LIS–WRF simulations and model specifications for these experiments can be found in S09.

As was performed for the IHOP-02 experiments in S09, each of the LSMs were run for an approximately four-year period prior to the start time of the IHOP-02 period to create equilibrated, or spun up, land surface states for initialization of LIS–WRF. These runs were performed offline (uncoupled) in LIS, using best-available atmospheric forcing data. Figure 2 shows the upper layer (0–10 cm) soil moisture values over the 1-km resolution domain as generated by the Noah and CLM spinup runs valid at 1200 UTC 12 June 2002. Also shown are the dry and wet soil sites from S09 and Fig. 1, as well as the sites

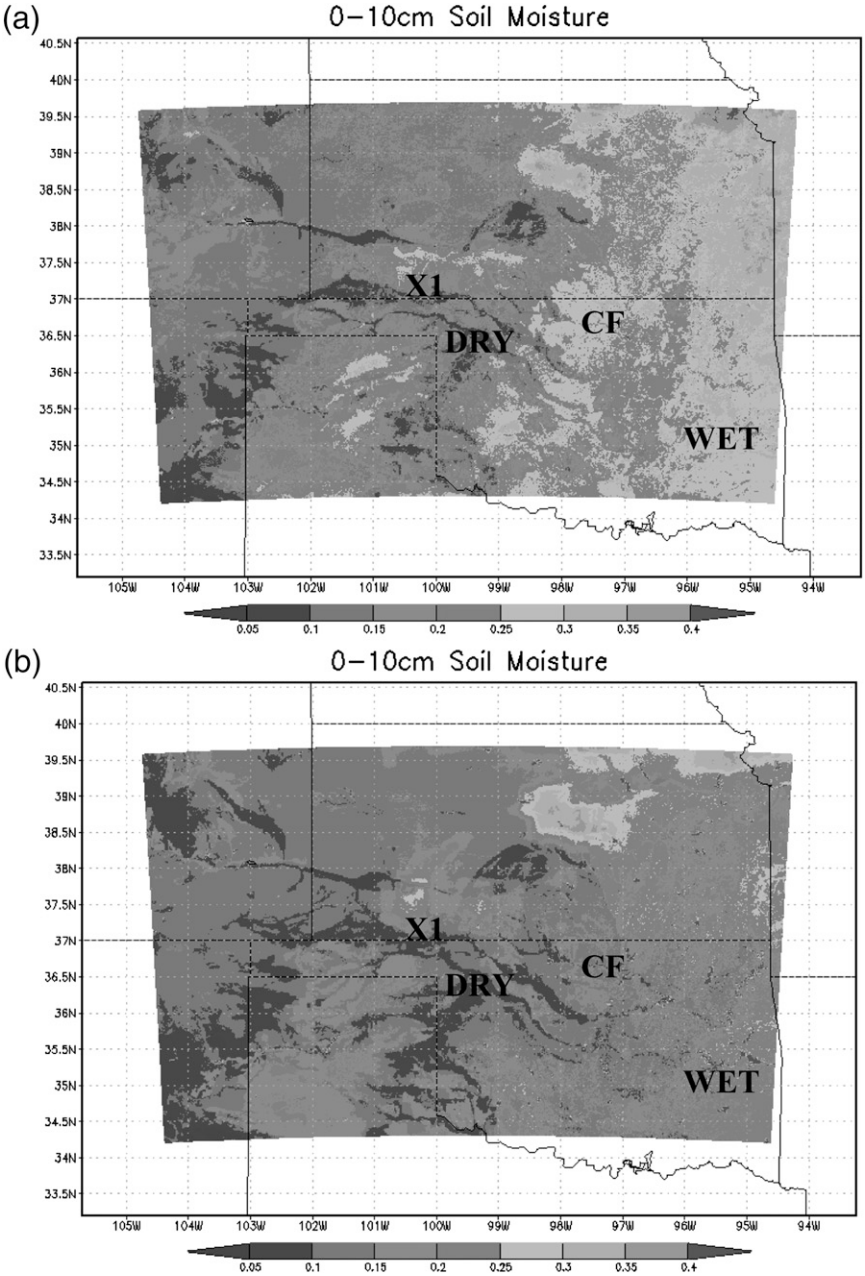

FIG. 2. Soil moisture ($m^3\ m^{-3}$) in the upper 0–10-cm layer valid at 0000 UTC 12 Jun 2002 as simulated from a 3.5-year spinup of the (a) Noah and (b) CLM models over the 1-km LIS–WRF domain in the SGP. The CF at Lamont, OK, and site X1 presented later in the results are also shown.

used in the analysis below. The advantages of using LIS for initialization are evident in the high spatial resolution seen in Fig. 2 as a reflection of the inputs of vegetation and soil properties for Noah and CLM versus the WRF default initialization (not shown). Using these spinup simulations as initial surface conditions, LIS–WRF simulations were then performed over a single, high-resolution domain (500×500; see Fig. 2), centered over the Oklahoma and Kansas border with a horizontal resolution of 1 km and time step of 5 s. The remainder of the model specifications remain identical to those in S09, including the vertical resolution and initial–boundary condition datasets.

4. Results

a. Thermodynamic extensions of S09 results

As outlined in section 2, LoCo as governed through the process chain in Eq. (4) can be diagnosed by utilizing

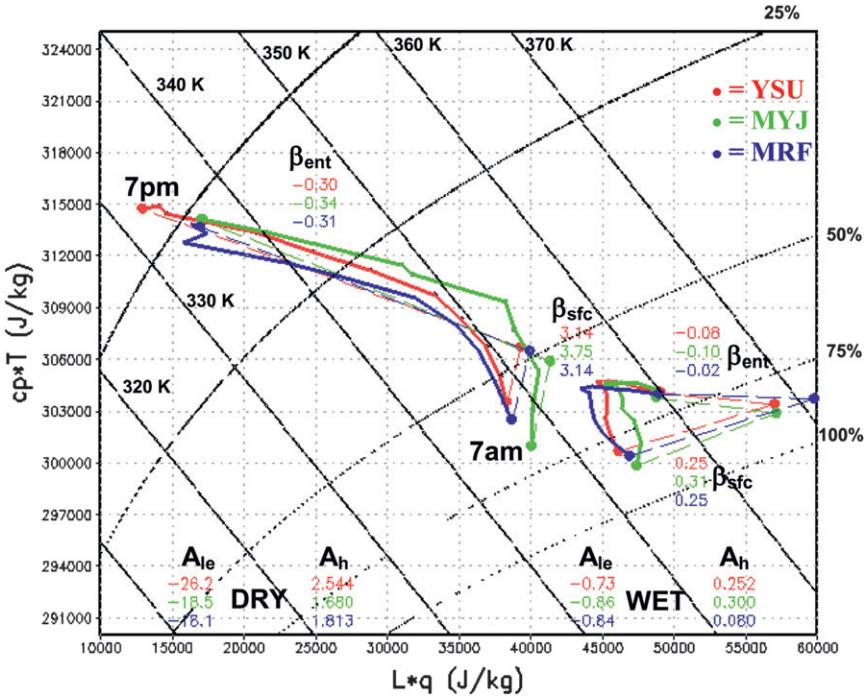

FIG. 3. Diurnal coevolution of 2-m specific humidity (Lq) and 2-m potential temperature ($C_p\theta$) on 12 Jun 2002 as simulated by LIS–WRF for (left) a dry soil (0.11 m^3 m^{-3}) and (right) a wet soil (0.30 m^3 m^{-3}) site in the Southern Great Plains using the Noah LSM with the YSU (red solid), and MYJ (green solid), and MRF (blue solid) PBL schemes (based on Figs. 3a, 5a from S09). Overlain are lines of constant θ_e (K; solid diagonal) and RH (%; dashed curved). Also shown are the surface ($\mathbf{V}_{sfc}$) and entrainment ($\mathbf{V}_{ent}$) vectors (dashed lines), surface (β_{sfc}) and entrainment (β_{ent}) Bowen ratio values, and heat (A_h) and moisture (A_{le}) entrainment ratios.

the thermodynamic properties (viz. θ_e, RH, P_{lcl}, and Δq^*) of mixing diagrams.

1) MOIST STATIC ENERGY AND RELATIVE HUMIDITY

An important measure of the potential for low-level heat and moisture to influence cloud development and precipitation is that of the moist static energy (MSE), or θ_e. Figure 3 shows the mixing diagram from the dry and wet soil site as simulated by the Noah LSM coupled to the three PBLs in LIS–WRF and presented in S09. When overlain with lines of constant θ_e, the tendency of MSE throughout the day can be easily quantified. For all three PBL–LSM couplings at the dry site, θ_e decreases by over 10 K throughout the day to values below 340 K. This is a direct result of weak surface evaporation (little moisture input), deep PBL growth (diluting mixed-layer properties), and strong dry entrainment flux (reducing moisture input) more than compensating for any PBL warming from the surface and entrainment. Also evident are the relative contributions of the surface flux (increasing θ_e) and entrainment flux (decreasing θ_e) vectors to the change in MSE, which in this case reduces the potential for clouds and convection over dry soils.

In contrast, the wet soil site shows an increase in θ_e by more than 5 K for each of the simulations to values near 350 K. This buildup in MSE is a result of strong surface evaporation, a slowly growing and shallow PBL, and more limited entrainment than the dry soil site. The surface vector ($\mathbf{V}_{sfc}$) is nearly perpendicular the lines of θ_e, indicating that the contribution to increasing MSE is dominated by the surface heat and moisture fluxes. On the other hand, β_{ent} values are <-0.10 indicating that dry air dominates over heat entrainment and acts to somewhat limit the MSE buildup over wet soils. In Fig. 3, RH has also been overlain for reference. It follows that at the dry site the low-level RH decreases from about 60% to 12.5%, while at the wet site it only decreases from 75% to 65%. Also note that at the wet site $\mathbf{V}_{sfc}$ is nearly parallel to the lines of constant RH (75%), indicating that the surface fluxes alone act to maintain a consistently moist PBL throughout the day. The implications of this 2-m RH tendency will be discussed in more detail in section 5.

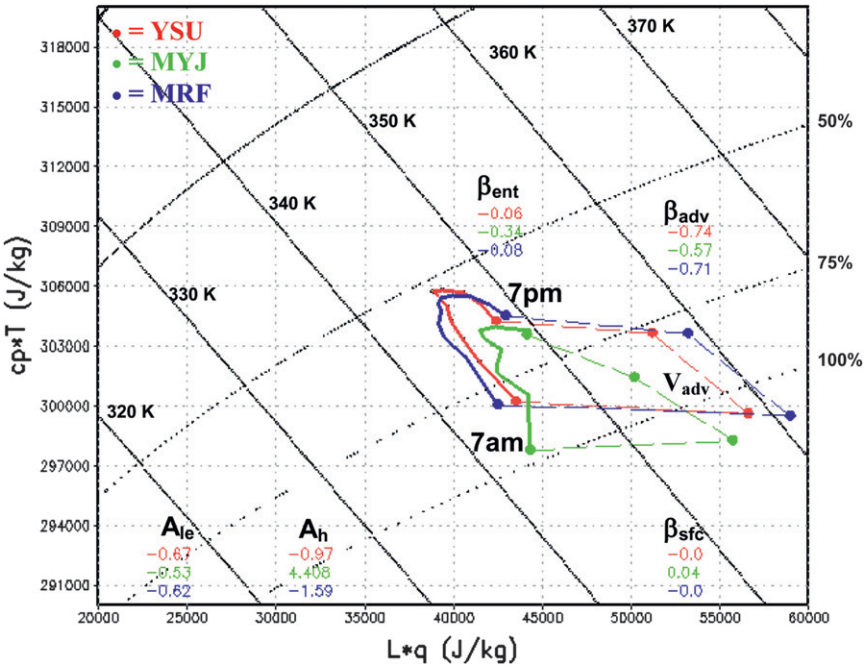

FIG. 4. As in Fig. 3 at the wet soil site, but for simulations using CLM and with the addition of the advection vectors (based on Fig. 13b of S09).

2) ADVECTION STRATIFICATION

With regards to sites impacted by advection, Fig. 4 shows the mixing diagram for the wet soil site in Fig. 3 for simulations using CLM coupled to the three PBLs in LIS–WRF. As presented in S09, this is a site that exhibited significant horizontal advection that could be included in Fig. 4 as a third vector ($\mathbf{V}_{\mathrm{adv}}$) with component fluxes of heat (H_{adv}) and moisture (LE_{adv}). In the context of MSE, it is noteworthy that the evolution of θ and q for a majority of the day runs parallel to the lines of constant θ_e (~345 K) despite having a strongly evaporating surface. In this case, θ_e increases by less than 5 K while RH decreases by more than 20%. This is in response to the warm and dry advection fluxes being significant and preventing the MSE from building up as strongly as it would have otherwise.

From a broader perspective, the issue of horizontal advection is one that should be considered using the mixing diagram approach but at the same time complicates the diagnosis of LoCo. Advection, by definition, causes LA interactions and coupling to be less local depending on its magnitude. While the results of S09 were presented at sites with minimal advection (with the exception of the CLM wet soil site shown in Fig. 4), this certainly cannot be assumed the case for other sites, experiments, and models. Therefore, using the PBL heat and moisture budgets derived from mixing diagrams, a metric is defined that quantifies the influence of advection on the LA coupling as follows:

$$\mathrm{AR}_H = \frac{H_{\mathrm{adv}}}{H_{\mathrm{sfc}} + H_{\mathrm{ent}}} \tag{9}$$

$$\mathrm{AR}_{LE} = \frac{LE_{\mathrm{adv}}}{LE_{\mathrm{sfc}} + LE_{\mathrm{ent}}}, \tag{10}$$

where AR_H and AR_{LE} are defined as the advective flux ratios. In effect, these ratios indicate the strength of advection relative to the combined surface and entrainment contribution to the full PBL budgets of heat and moisture, and as such their magnitudes suggest how local the LA coupling actually is for each. When applied to the dry, intermediate, and wet soil sites from S09, the values of AR_H and AR_{LE} in Table 1 confirm that the LA coupling was primarily local for all sites and models, with the exception of the warm and dry advection exhibited by CLM at the wet site. It is also important to note that advection vectors for the remaining sites presented in this paper were also found to be rather minor components ($\mathrm{AR} < 0.10$), and therefore for the sake of clarity were omitted from the figures and discussion.

3) MOIST PROCESSES AND PRECIPITATION

Although the analyses presented in S09 and Figs. 3 and 4 focus on primarily clear-sky locations during IHOP-02,

TABLE 1. Advective flux ratios for heat (AR_H) and moisture (AR_{LE}) calculated from Eqs. (8) and (9) for LIS–WRF simulations using the Noah and CLM LSMs with the YSU, MYJ, and MRF PBL schemes. The ratios were derived using the mixing diagram theory and surface, entrainment, and advection flux vectors for the dry, intermediate, and wet soil sites (Fig. 3) presented in S09.

DRY	AR_H	AR_{LE}
Noah-YSU	0.10	0.14
Noah-MYJ	0.06	0.19
Noah-MRF	0.06	0.08
CLM-YSU	0.05	0.05
CLM-MYJ	0.02	0.10
CLM-MRF	0.03	0.01
INT	**AR_H**	**AR_{LE}**
Noah-YSU	0.04	0.02
Noah-MYJ	0.09	0.01
Noah-MRF	0.06	0.04
CLM-YSU	0.04	0.05
CLM-MYJ	0.04	0.08
CLM-MRF	0.05	0.08
WET	**AR_H**	**AR_{LE}**
Noah-YSU	0.23	0.03
Noah-MYJ	0.18	0.01
Noah-MRF	0.31	0.08
CLM-YSU	3.36	0.25
CLM-MYJ	1.22	0.32
CLM-MRF	2.86	0.22

the 12 June case also contained a portion of localized clouds and precipitation in the SGP domain and is therefore of particular interest for convective initiation studies. Figure 5a shows the mixing diagram for the Noah simulations at a different wet soil location where convective precipitation occurs in the late afternoon. While the concept behind mixing diagrams does not easily extend to such conditions because of complications involved with saturated processes, latent heat release, and most importantly the breakdown of surface fluxes and PBL itself, they can still be used as a tool to evaluate the buildup and fueling of convection.

At this site, the morning buildup of MSE is higher ($\theta_e >$ 350 K) than that seen at the wet site in Fig. 3. This acts to lower both the lifting condensation level (LCL) and the level of free convection (LFC), both of which were able to be reached by the growing PBL to cause the formation of clouds by midday and precipitation by late afternoon. The rapid cooling of the PBL following the rainfall is seen in the plots, which also show the associated increase in RH expected after the 2-m temperatures drop and the air becomes nearly saturated.

The CLM simulations at this site (Fig. 5b) also produce clouds and precipitation, but show more sensitivity to the PBL coupling. For example, the YSU and MRF schemes result in θ_e increasing to near 365 K by midday, while the MYJ scheme reaches 355 K (note that θ_e values are higher than the corresponding Noah simulations). This is due to more rapid and early PBL growth by the MYJ scheme (not shown), which acts to dilute some of the MSE buildup, whereas YSU–MRF exhibit slower growth and act more as a lid on the surface heating and evaporation into the PBL. The development of clouds and precipitation then follows where YSU–MRF triggers deeper and earlier convection as seen in the cloud vertical profiles than the simulation with CLM coupled to MYJ. It should be noted that advection is minimal in Figs. 5a and 5b, and the site is located in a relatively homogeneous region of wet soil conditions (see Fig. 2 for Noah and CLM), thereby also supporting the buildup of high MSE.

b. *Soil moisture perturbation experiments*

1) POTENTIAL SATURATION HUMIDITY DEFICIT

By overlaying Δq^*, the relative saturation of the PBL can also be easily evaluated using mixing diagrams. As discussed in section 2, this is related to the concept of equilibrium evaporation [defined as constant $d(\Delta q^*)/dt$] when the PBL reaches a level of constant saturation deficit in response to the moisture entering the PBL from evaporation and that exiting through entrainment and/or advection. Therefore, the degree to which a change in soil moisture impacts the tendency toward or away from PBL equilibrium can be diagnostic of the role of the land surface in the LoCo process chain.

To investigate this, a new set of experiments was conducted for the IHOP-02 cases by perturbing the initial soil moisture states in the LIS–WRF simulations. From the offline Noah spinups, the soil moisture was uniformly (both horizontally and vertically) perturbed to both a wet ($+0.10$ m^3 m^{-3}) and dry (-0.10 m^3 m^{-3}) condition with which to initialize the coupled model and evaluate against the default simulation. The impact of ΔSM on a particular PBL–LSM coupling (Noah + YSU) at site X1 is summarized in the mixing diagram shown in Fig. 6a. What is most evident is the impact of soil moisture on the daytime evolution of θ and q, particularly for the wet perturbation simulation. Surface evaporation limits the large growth of the PBL seen the dry and default runs, which results in a much smaller entrainment vector. Other than a 1-h period of slowed PBL growth in the dry simulation (as it was growing through a stable layer), the default and dry runs are markedly similar in their diurnal mean temperature and moisture evolution as well as surface and entrainment fluxes.

In terms of the saturation deficit, the dry and default runs nearly continuously dry out throughout the day farther away from saturation. However, the wet simulation reaches a point in early afternoon where it ceases

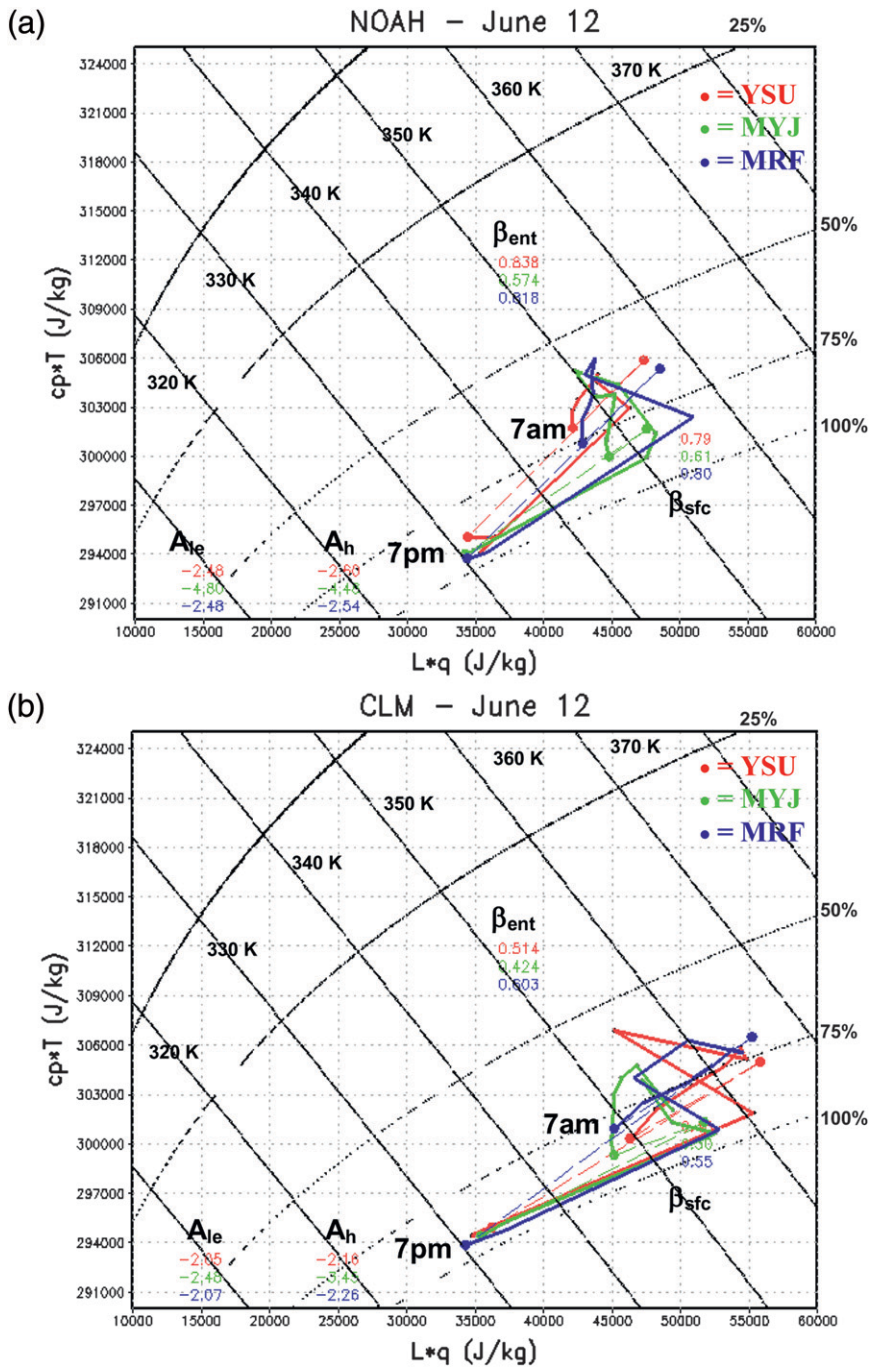

FIG. 5. (a) As in Fig. 3a, but for a different wet soil site (0.31 $m^3\ m^{-3}$) in the ARM–SGP domain (lat = 38.2, lon = −95.4) where convective precipitation was simulated from 2100 to 2300 UTC. (b) As in (a), but for simulations using CLM.

to dry out and follows a constant Δq^* (~.023 kg kg^{-1}) for the remainder of the day. This follows the theory of an equilibrium condition being reached (as can happen over very wet surfaces), and can be explained through the mixing diagram information as follows.

In all three simulations, the first half of the day is dominated by PBL growth, dry air entrainment, and increasing temperature in the PBL, all three of which tend to increase the saturation deficit. The wet simulation has less surface heating to drive PBL growth, however, and

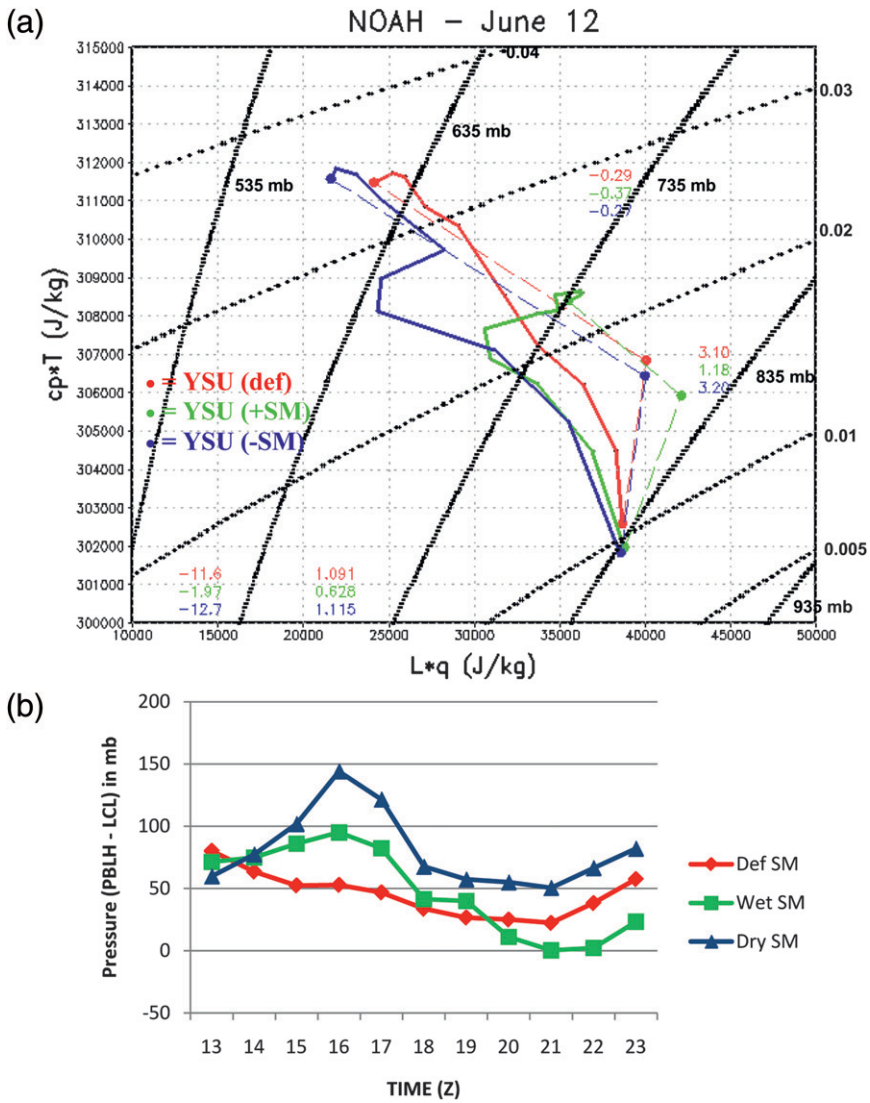

FIG. 6. (a) Diurnal co-evolution (1200–0000 UTC) of 2-m specific humidity (Lq) and 2-m potential temperature ($C_p\theta$) on 12 Jun 2002 as simulated by LIS–WRF at site X1 (lat = 37.101, lon = −100.200) in the Southern Great Plains using the Noah LSM with the YSU PBL scheme and initialized with default (red solid), wet (green solid), and dry (blue solid) soil moisture perturbations. Overlain are lines of constant Δq^* (kg kg^{-1}; dotted) and P_{lcl} (mb; solid diagonal), and the vectors and derived metrics as in Fig. 3a. The initial soil moisture values for the 3 simulations are 0.19 m^3 m^{-3} (default), 0.29 m^3 m^{-3} (positive), and 0.09 m^3 m^{-3} (negative). (b) Difference between PBL height (mb) and P_{lcl} (mb; referred to as the LCL deficit) at each hour of the simulations shown in (a).

by the early afternoon its PBL growth slows considerably. After this point, a balance of the slight increase in temperature with the surface evaporation is reached and results in a constant Δq^*. In terms of diagnosing LoCo, the sensitivity of the coupled system [in terms of Eq. (4); $\Delta\theta$, Δq, ΔEF, ΔPBL, and ΔENT] to a change in soil moisture is evident through this analysis including the tendency toward a drying, moistening, or equilibrating regime as governed by Δq^*.

2) LIFTING CONDENSATION LEVEL

A necessary condition for clouds and precipitation to form is that P_{lcl} is reached by parcels contributing to the growth of the PBL, and as such the sensitivity and variability of P_{lcl} has proven to be a valuable diagnostic of LA coupling over a range of scales and conditions (Betts 2004). Because P_{lcl} is a direct function of low-level temperature and moisture, it too can be overlain on mixing diagrams

and its evolution can be evaluated against the actual growth of the PBL.

As discussed in the previous section, the wet perturbation in Fig. 6a results in a distinctly different diurnal behavior of the temperature and moisture states and fluxes at this site relative to the default and dry runs. In terms of P_{lcl}, this results in a significantly lower altitude (higher pressure) of the lifting condensation level after midday in the wet simulation, with the default and dry runs reaching values of P_{lcl} very high into the troposphere. In fact, values of 600 mb indicate that parcels, and in effect the PBL height, would have to reach well over 3 km into the atmosphere during the PBL growth to reach the saturation point governed by the P_{lcl}. This is a result of the consistent drying out of the PBL in the default and dry runs that is caused by entrainment and dilution of heat and moisture within a deep and well-mixed PBL. Conversely, the near-equilibrium evaporation condition reached during the wet simulation actually results in a slight rise in P_{lcl} during the late afternoon, meaning the PBL need not grow nearly as high to reach saturation.

When compared against the diurnal evolution of PBL height, the ability of parcels to reach the condensation level can be directly evaluated. Figure 6b plots the hourly differences in PBL height and P_{lcl} (hereafter referred to as the LCL deficit) for each of the perturbation simulations, and shows that the ability of the PBL to reach the condensation level is indeed sensitive to the initial soil moisture. The dry run remains at least 50 mb short of reaching P_{lcl}, while the wet perturbation results in the P_{lcl} nearly being reached late in the afternoon. It usually takes deeper and prolonged penetration of the PBL through the P_{lcl} for cloud formation, so all three simulations remained cloud-free at this site. However, it is important to point out that although the change in SM did not impact clouds or precipitation per se, it still did impact the coupled system and LoCo process chain in a significant manner (discussed below in terms PBL budgets).

Figure 7a shows the mixing diagram with P_{lcl} overlain at the ARM-SGP Central Facility (CF). Once again, the default (0.30 $m^3\ m^{-3}$) and dry (0.20 $m^3\ m^{-3}$) runs are rather similar while the wet perturbation (0.40 $m^3\ m^{-3}$) results in somewhat limited temperature and moisture evolution as a result of higher evaporative flux and slower, shallower PBL growth. In addition to not reaching an equilibrium evaporation condition, this location differs from the site in Fig. 6a in that the P_{lcl} values are much higher (lower altitude, <3 km) in each simulation. As a result, the PBL height reaches and consistently exceeds the P_{lcl} in late afternoon resulting in a sustained negative LCL deficit for all three simulations (Fig. 7b). The default simulation is sufficiently wet such that both dry and wet perturbations evaporate strongly enough to support a PBL evolution that results in corresponding cloud formation in all three runs in the late afternoon (Fig. 7c). In turn, the LoCo components of Eq. (4) support only a very limited sensitivity of clouds and precipitation to the initial soil moisture perturbation at this site.

3) Spatial analysis of LCL deficit

The LCL deficit can also be analyzed spatially to evaluate the sensitivity of regional-scale PBL, cloud, and precipitation development to soil moisture perturbations. Figure 8 shows the LCL deficit for the full LIS–WRF domain valid at 2100 UTC for each of the perturbation simulations. Negative values (LCL deficit < 0) indicate that the PBL has grown to at least the P_{lcl}, with the most strongly negative values most likely to support sufficient lift and condensation for cloud formation. In comparing the three plots, it is apparent that the wet simulation (Fig. 8c) results in a broader area of positive LCL deficit that supports clear skies, while the dry run (Fig. 8b) actually promotes regions of more strongly negative values and therefore greater potential for cloud formation. This supports the idea of a negative feedback of soil moisture on clouds and precipitation (as discussed in section 2) for dry soil perturbations. There are also locations where the reverse (i.e., wet perturbation increasing the likelihood of clouds) takes place, but do not represent the dominant signal of the impact of the perturbation seen here.

If we zoom in on the feature in the center of the domain just east of the Oklahoma panhandle and isolate only the negative LCL deficit values (Figs. 9a,c,e), we can examine more closely the impact of the soil moisture perturbations. All three plots indicate that the PBL height has reached the P_{lcl} at similar locales; there are distinct differences in the magnitude of the negative LCL deficit reached in the wet and dry runs, with the dry runs showing more strongly negative values in the southwest (SW)–northeast (NE)-oriented line. When comparing directly against the integrated cloud liquid water in each run (Figs. 9b,d,f), it is confirmed that the dry simulation results in significant cloud cover and precipitation (not shown) along that line while the wet simulation remains clear.

The processes governing these interactions and feedbacks can be explained as follows. The dry simulation was able to increase the buoyancy enough via increased surface heating to promote PBL growth that more than offsets the corresponding rise in P_{lcl} due to warm–dry air entrainment and lower near-surface humidity. Conversely, the wet simulation has limited PBL growth to such as degree that it cannot reach the P_{lcl}, even after having been lowered due to reduced warm–dry entrainment and higher near-surface humidity. [Note also that this is a snapshot in time (2100 UTC), and full assessment of daytime

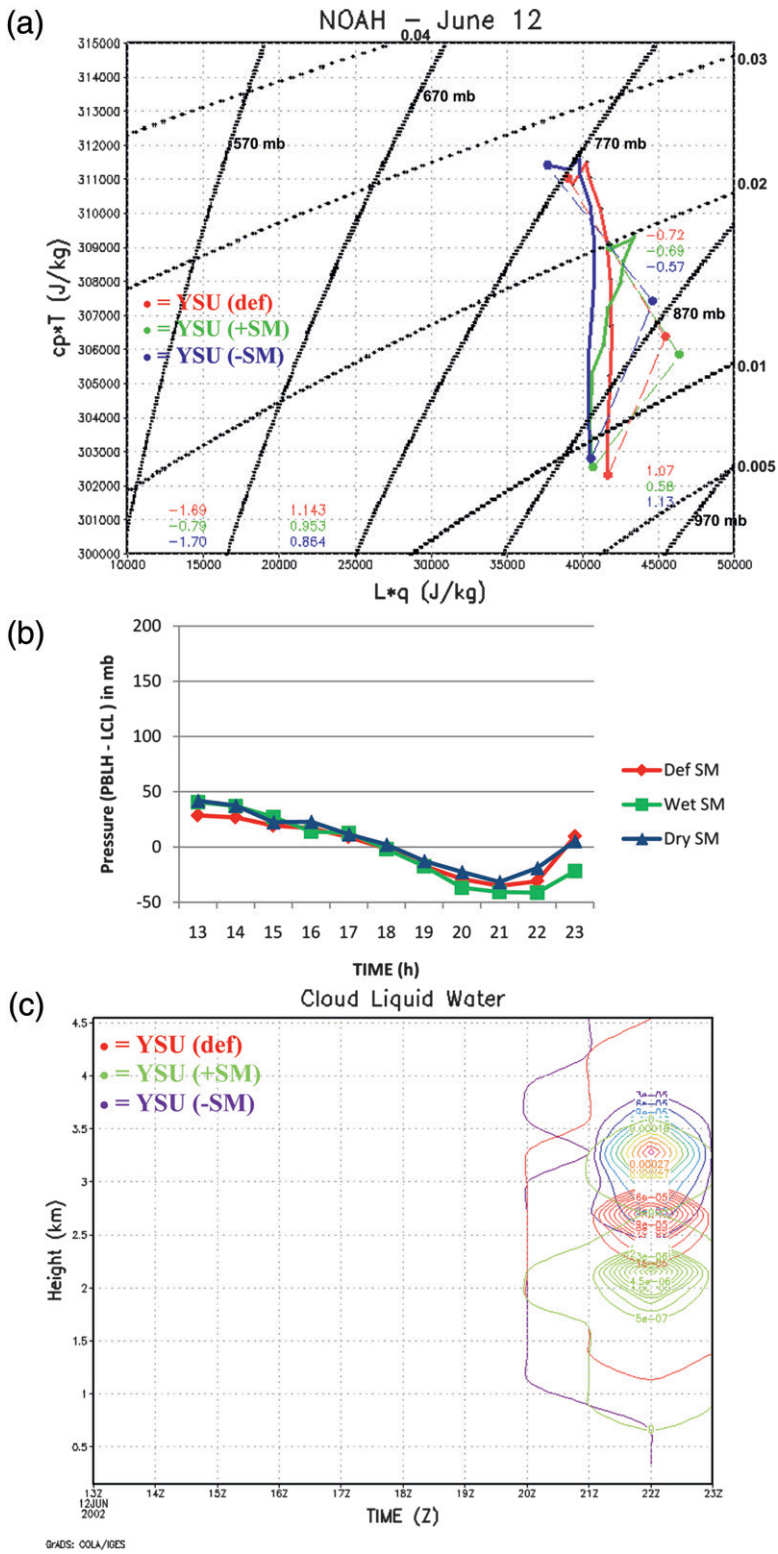

FIG. 7. (a) As in Fig. 6a, but at site CF (lat = 36.605°, lon = −97.485°). The initial soil moisture values for the three simulations are 0.30 $m^3\ m^{-3}$ (default), 0.40 $m^3\ m^{-3}$ (positive), and 0.20 $m^3\ m^{-3}$ (negative). (b) LCL deficit (mb) at each hour of the simulations shown in (a). (c) Time series of vertical cloud liquid water profiles (g kg^{-1}) for each of the perturbation runs at the ARM-SGP CF site in (a).

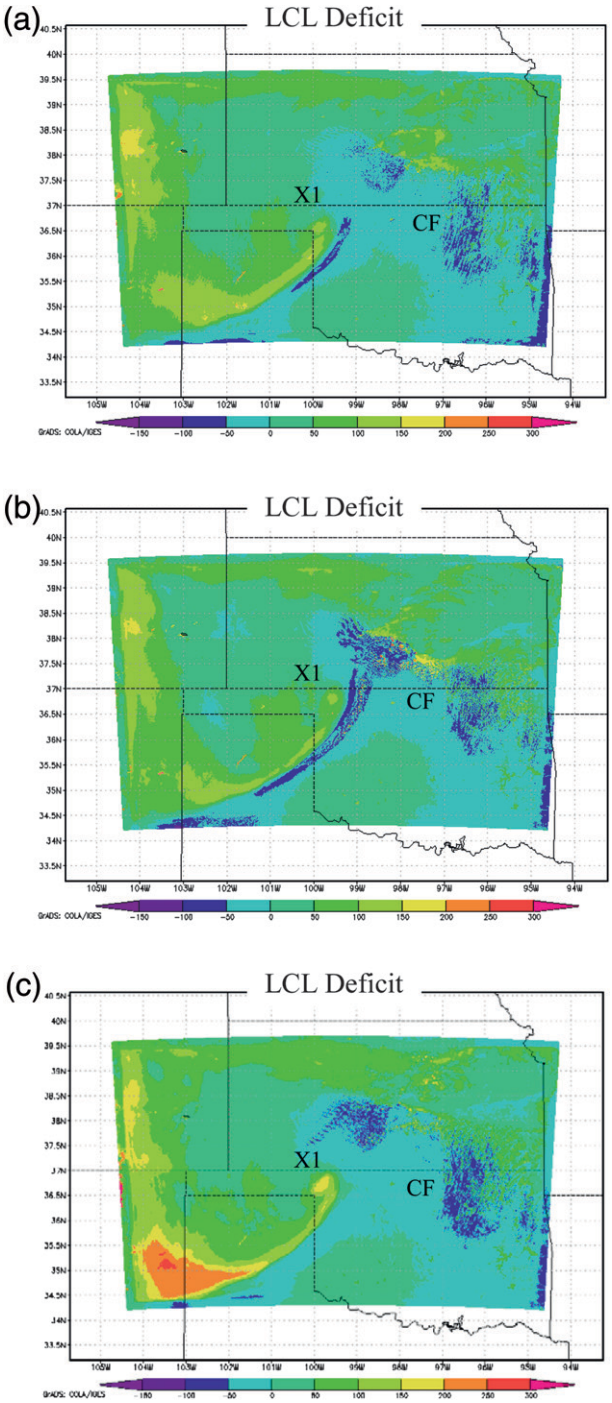

FIG. 8. The LCL deficit (mb) for the full SGP domain at 2100 UTC for the (a) default, (b) dry, and (c) wet soil moisture perturbation simulation employing the Noah LSM and YSU PBL scheme.

convection would require integration over the afternoon period as well as moving horizontally with the advective flow. Therefore an exact 1:1 spatial correlation on the grid scale (1 km) is not expected.]

c. *Integrative LoCo diagnostics*

1) PBL BUDGETS

As shown in S09, the mixing diagram approach to diagnosing LoCo also includes analysis of the full PBL budgets of heat and moisture as derived quantities from the diagrams themselves. Figure 10 shows the sensible and latent heat fluxes for each component of the PBL budgets for the perturbation simulations at the two sites in Fig. 6 and Fig. 7. At site X1, the wet perturbation is reflected in lower H and higher LE (i.e., lower Bowen ratio), and lower surface available energy than the default and dry runs. What is most evident is the large magnitude of the entrainment fluxes of the default and dry runs, with both dry and warm air fluxes 3–4 times that of the wet perturbation due to the limited PBL growth. The near-balance of evaporation with dry air entrainment in the dry run is also seen in the total PBL budget value of LE being much closer to zero than the other two simulations.

In contrast, site CF shows much lower and more comparable range of magnitudes across all of the PBL budget components because of reduced PBL growth in all simulations. Similar to site X1, the impact of the wet perturbation is seen in a lower Bowen ratio but in this case the available energy is sensitive to the wet perturbation while the dry run remains close to the default value (likely because of interaction of soil albedo and soil heat flux variability). The entrainment fluxes are diminished in the wet run, though much less so than at site X1, and the total PBL budgets are warmer and drier in the default and dry runs, while the wet run results in a net moistening of the PBL.

Overall, the components of the PBL budgets help to determine the overall heat and moisture balance of the coupled system, and how a soil moisture perturbation impacts these balances. Results from these two sites show that soil moisture tends to have greater impact on LoCo and cloud development when PBL growth, including its potential and its sensitivity, is large thereby allowing for entrainment feedbacks to play a significant role. It is also important to note that the impact of soil moisture variability can still be significant and felt through the LoCo chain in Eq. (4) without resulting in clouds or precipitation (e.g., Figs. 6a,b and Fig. 10a), and is quantified most readily through these PBL budgets in terms of the change in LA fluxes.

2) EVAPORATIVE FRACTION VERSUS PBL HEIGHT

An additional analysis that can be derived from the mixing diagram approach is shown in Fig. 11, which presents the relationship between mean evaporative fraction and maximum PBL height for each of the perturbation simulations at the two sites above. While previously shown

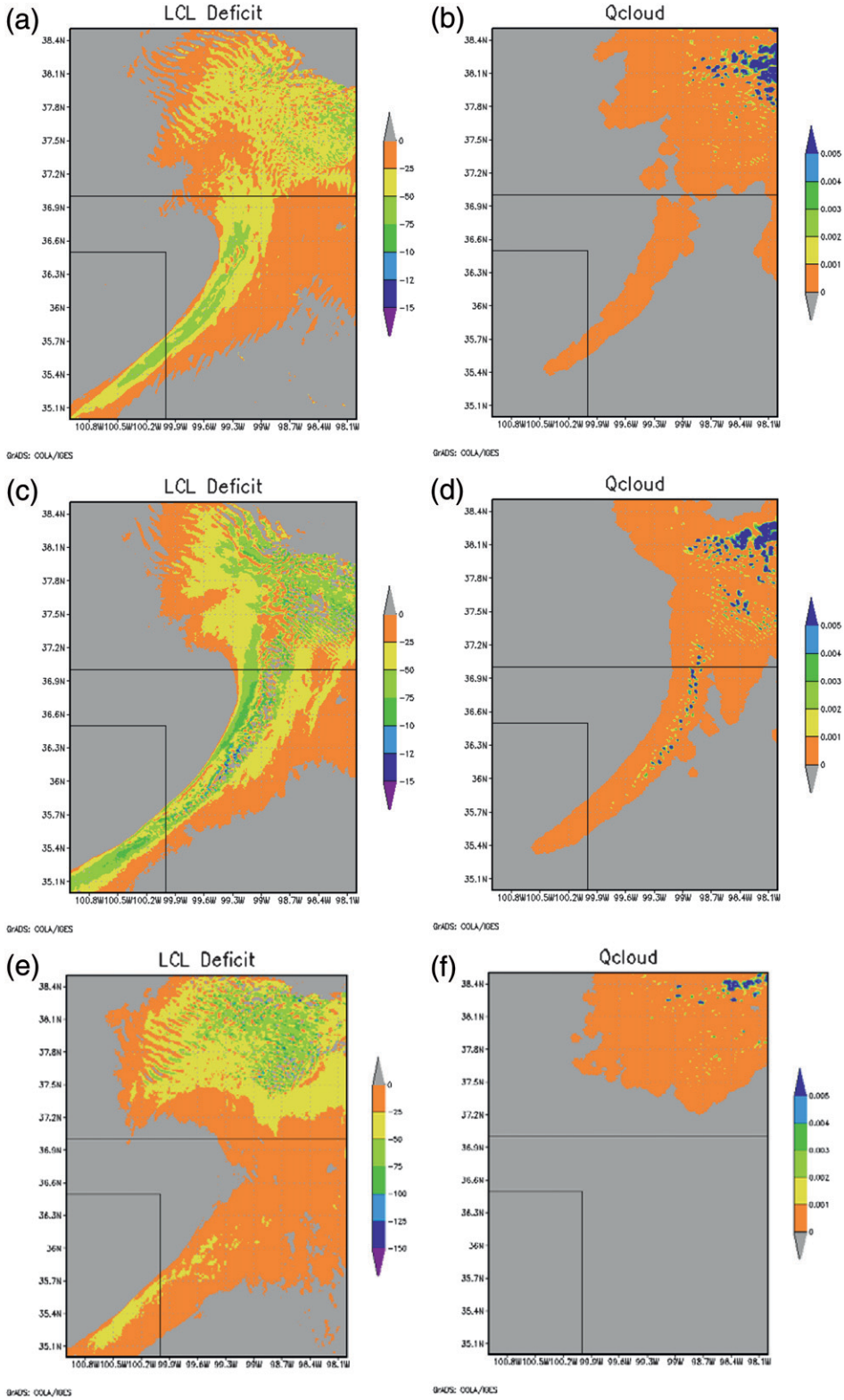

FIG. 9. The LCL deficit (mb) for the (a) default, (c) dry, and (e) wet soil moisture perturbations, and vertically integrated cloud liquid water (g kg^{-1}) for the (b) default, (d) dry, and (f) wet soil moisture perturbations valid at 2100 UTC over a subset of the full ARM-SGP domain.

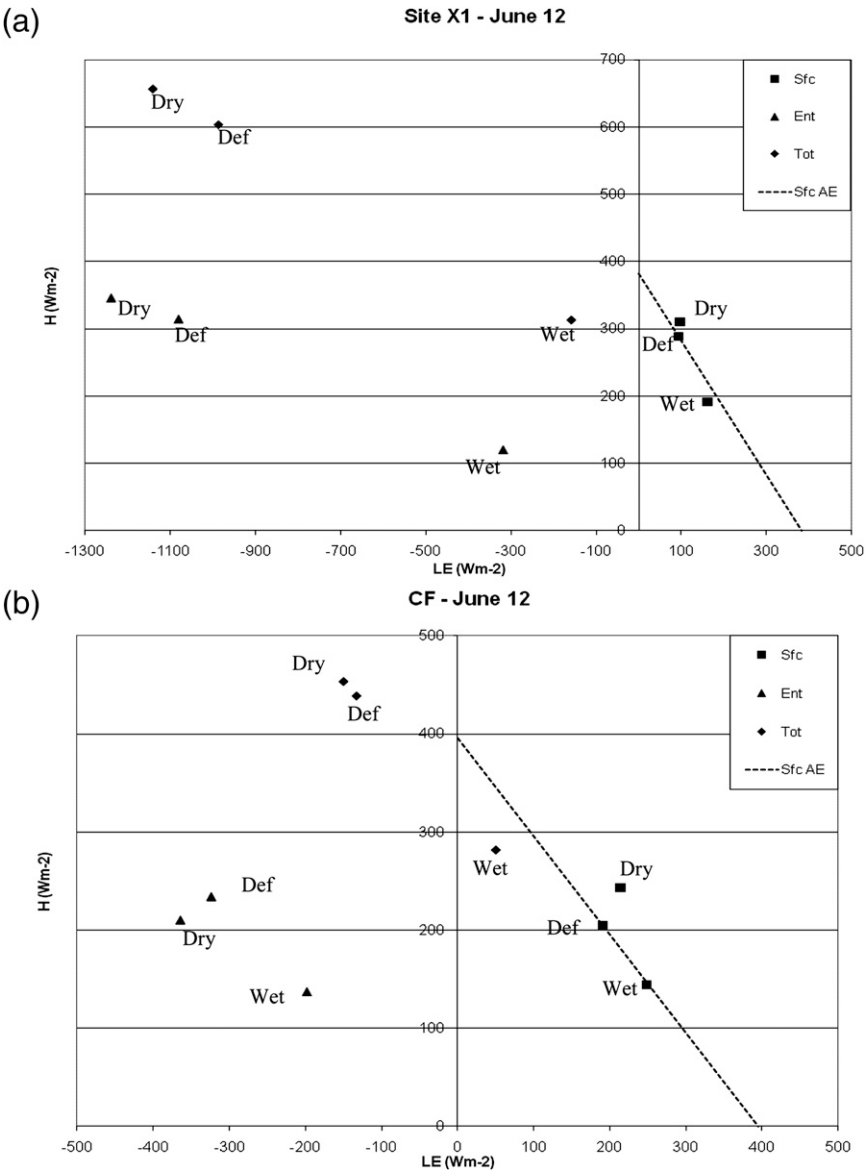

FIG. 10. Fluxes of latent (LE; W m^{-2}) vs sensible (H; W m^{-2}) heat from the land surface (squares), entrainment (triangles), and the total PBL budget (diamonds) simulated by the LIS–WRF perturbation simulations at the sites shown in (a) Figs. 6a,b and (b) Figs. 7a,b. The dashed line shows the total surface available energy based on the default soil moisture simulation.

by S09 to be useful in stratifying the relative sensitivity of PBL and LSM choices, the impact of soil moisture perturbations can be evaluated here in terms of the bulk impact on the surface (ΔEF) and the atmosphere (ΔPBL), both critical components of the LoCo feedback chain. In Fig. 10, the larger impact of the wet perturbation on the land and PBL state is apparent relative to the dry perturbations, which lie nearly on top of the default values.

In fact, the slope of a line connecting the default and perturbed simulations gives an indication of the sensitivity of the PBL evolution to the change in surface fluxes resulting from variations in SM. Here, the slopes of these lines from the default to the wet perturbations are 5250 m (1050 m/0.2) and 3333 m (500 m/0.15) for site X1 and site CF, respectively. Larger slopes indicate a greater PBL sensitivity to soil moisture relative to changes in EF, while smaller values suggest that the surface fluxes are more strongly impacted by a change in soil moisture than is the PBL itself. This approach can be used to indicate what locations and conditions (e.g., soil moisture range) show stronger potential for strong coupling (site X1) than others (site CF). Further, if a broader

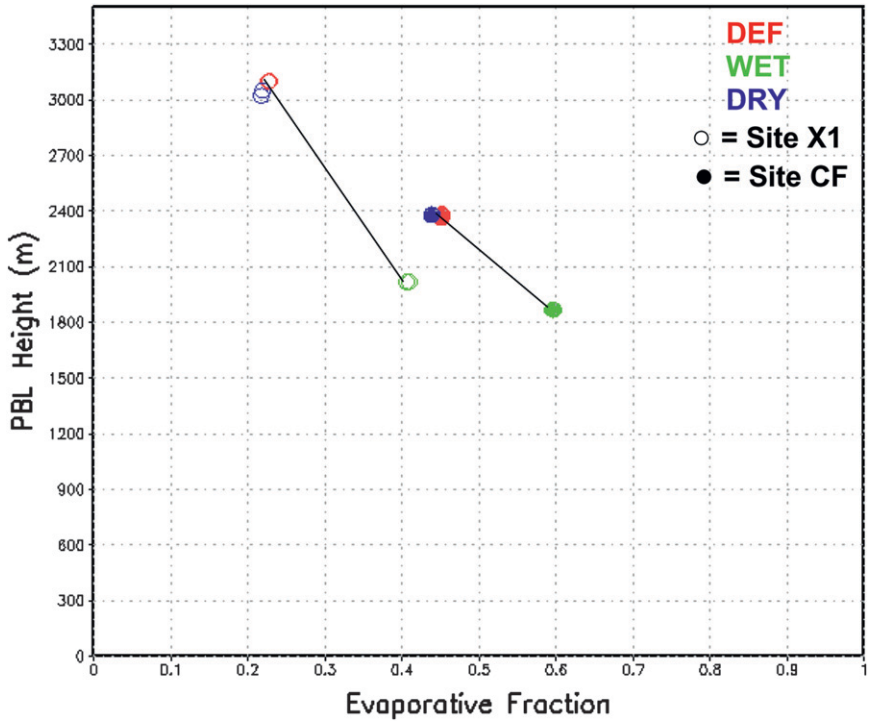

FIG. 11. Daytime mean evaporative fraction (−) vs maximum PBL height (m) for the default (red), wet perturbation (green), and dry perturbation (blue) LIS–WRF simulations for the sites shown in Figs. 6a,b (open circles) and Figs. 7a,b (closed circles). Also shown are lines (dashed) used to calculate the slope of the default vs wet perturbation values at each site.

range of soil moisture perturbations are simulated at fine intervals, a curve describing the impact of ΔSM on ΔEF and ΔPBL could be defined across the soil moisture spectrum at each site.

5. Discussion and conclusions

The complexity of LA interactions requires the full components [i.e., Eq. (4)] of the coupled system to be evaluated simultaneously in order to diagnose the sensitivity of the PBL, clouds, and precipitation to the land surface condition. To this end, we have demonstrated how extensions of the mixing diagram approach presented in S09 can be used as a comprehensive analysis framework for addressing LoCo and its inherent sensitivities. These extensions include thermodynamic overlays, advective ratios, and the LCL deficit. Using the LIS–WRF system, the analysis has been applied to results from simulations with varying LSM and PBL scheme couplings and initial soil moisture conditions.

The coevolution of temperature, humidity, PBL growth, and surface fluxes has been integrated and evaluated in terms of their thermodynamics using mixing diagrams. Specifically, overlays of RH and θ_e and their time tendencies during the day define how each PBL–LSM coupling evolves toward a drier or moister state with respect to temperature, and can therefore assess the potential for fueling convection as defined by the MSE. Mixing diagrams, previously only presented for clear-sky cases, have thus been extended to include locations–conditions where moist processes (i.e., PBL clouds and precipitation) are dominant. At these sites, the θ_e tendency in particular is shown to be a key determinant of whether a particular PBL–LSM coupling results in clouds and/or precipitation. The importance of near-surface θ_e has also been shown to be a determinant in the type of convection (intense versus nonintense), so the utility of this analysis may not be limited to triggering alone (Nicholls and Mohr 2010).

The relationship between the near-surface RH evaluated here and the RH-tend formulation for the top of the PBL as developed by Ek and Holtslag (2004) is something that calls for further investigation. While RH-tend is more explicit and formal in describing entrainment, PBL heating, and PBL growth, it is clearly more difficult to specify the full set of terms as opposed to the simpler mixing diagram approach. The degree to which the near-surface RH and the RH-tend are correlated may enable a connection to be made between the surface and PBL top and therefore insight on the SM–P relationship. Currently,

work is underway to develop sensitivity expressions for SM-RH-tend and EF-RH-tend that also attempt to link the surface to the full PBL interaction.

Along the same lines, the results here tie directly to the work of De Ridder (1997) in assessing the EF–PBL relationship and the potential for fueling convection. Because $d\theta_e/d\mathrm{EF}$ can be calculated directly from mixing diagrams, the sensitivity of MSE to the surface moisture condition can be calculated without the need for assumptions about the PBL growth, entrainment, or the surface available energy (as was required in their approach), as these are already explicitly accounted for in the LIS–WRF simulations and reflected in the diagrams. Ultimately, the results of De Ridder (who used a slab model with many assumptions to obtain a full range of sensitivities) can be tested against results from a fully coupled model (such as LIS–WRF) and compared with observations to gain a sense for the true nature of the EF–PBL sensitivity its accuracy within the models themselves.

We have also shown how horizontal advection can be incorporated into the LoCo analysis such that 1) its contribution to the overall PBL budget can be quantified using an advective flux ratio, and 2) the sensitivity of the thermodynamics to advection can be assessed. It is critical that, if significant, advection be accounted for in the diagnostics of local coupling to ensure the PBL response is to the local land surface rather than a synoptic disturbance or large fetch over heterogeneous terrain.

Results from new LIS–WRF simulations that specify initial soil moisture perturbations have been presented in the context of two additional thermodynamic overlays, Δq^* and P_{lcl}. The potential saturation deficit has been linked to the concept of equilibrium evaporation, and when applied to mixing diagrams the tendency of a particular LA coupling toward or away from a balance in PBL moisture can be quantified. The sensitivity of $d(\Delta q^*)/dt$ to the initial SM is thus indicative of what degree the coupled system (and PBL) is sensitive to the land surface condition, and whether that tendency is toward a runaway drying and growing PBL regime or an EF–ENT balance that limits PBL growth and/or supports cloud and precipitation development.

Likewise, the LCL deficit can be calculated from P_{lcl} overlain on mixing diagram along with the actual growth of the PBL. This deficit is integrative of the impact of varying soil moisture and evaporation conditions on the PBL as a whole, including the ability of the PBL growth to reach the P_{lcl} (as determined from near-surface temperature and humidity). The impact of dry or wet SM perturbations on the LCL deficit was examined both diurnally and spatially, enabling the tendency of the coupled system to generate clouds and precipitation to be evaluated. It is notable that individual positive and negative feedbacks that govern the SM–P relationship can be directly identified here, which requires the high temporal and spatial scales of these LoCo experiments. This analysis also addresses the LoCo-scale (diurnal process level) component of the larger-scale model evaluation of the correlation between SM and P_{lcl} performed by Betts (2004).

In the perturbation experiments, it should be noted that the value of the default soil moisture is critical in determining the range of soil moisture relative to saturation and the wilting point that is ultimately captured. At site X1, the default (0.19 $\mathrm{m^3\ m^{-3}}$) and dry (0.09 $\mathrm{m^3\ m^{-3}}$) perturbations are in a soil-limited regime while the wet simulation (0.29 $\mathrm{m^3\ m^{-3}}$) is atmospherically controlled and freely evaporating, each determined by the particular LSM (in this case Noah), soil properties, and physics employed therein. This explains the similarity between the default and dry runs in Fig. 6a, and the tendency toward equilibrium evaporation for the wet simulation. To more directly account for this when considering the behavior of different LSMs and their evaporation schemes, future work will explore perturbations of the surface condition through stomatal resistance, for example, rather than absolute soil moisture values. This will also enable the sensitivities derived from Fig. 11 (i.e., through the slope measure) to be more comprehensively defined and quantified across the full soil moisture spectrum.

A promising next step in extending LoCo diagnostic work to cloud and precipitation regimes would be to diagnose the behavior, sensitivity, and impact of LoCo processes on the development of shallow (via the LCL deficit) versus deep convection as governed by the level of free convection (LFC). Zhang and Klein (2010) have developed an 11-year comprehensive analysis of land, PBL, and free-troposphere mechanisms that potentially impact (or favor) the development of shallow versus deep convection. Their results were also from the ARM-SGP region, and can therefore be placed directly in the context of the LoCo chain and surface flux and moisture sensitivities presented here.

Finally, we have tied together framework of S09 with the SM perturbation runs by evaluating the complete PBL budget and the relationship of EF-PBLH for each. The sensitivity of the surface, entrainment, and total PBL heat and moisture fluxes is indicative of how the surface condition impacts the mean PBL state and evolution, and can be directly linked with the tendency toward an equilibrium (or net flux) condition using Δq^*. Likewise, the relative sensitivities of EF and PBLH to a change in SM can be evaluated as the slope of perturbation values in the EF–PBLH space. This analysis can be related to the work of Jacobs et al. (2008), who defined the strength of surface layer (i.e., SM–EF) coupling as a function of the proportion of surface to aerodynamic resistance. Here, we

have extended this to include to the sensitivity of the full PBL and its feedbacks on the surface, and in effect LoCo, as well.

Overall, the diagnostic framework developed here and in S09 provides a methodology to evaluate the components of LoCo in their native and fully coupled environment using LIS–WRF. This same framework can also be applied to any modeling system and observations. While a quantification of LoCo using a single metric may not be possible because of the complexity of the process chain and feedbacks, the analyses presented here offer a blueprint for fully understanding each component in both an isolated and integrated sense. Particularly with the advent of next-generation satellite measurements of PBL and land surface properties for use in this context (e.g., Ferguson and Wood 2011) along with advances in land–atmosphere data assimilation schemes, the ability to evaluate and quantify LoCo within models will become even more of a priority for the hydrometeorological community.

To this end, the next phase of LoCo research will focus on the 2006–07 period of consecutive climatologically dry and wet years in the SGP region. These dry–wet ''extremes'' have also been chosen as a focal point for integration projects employing a new version of LIS–WRF with additional LSM and PBL options as a test bed by the NASA Energy and Water Cycle Study [NEWS; NASA Energy and Water Cycle Study (NEWS) Science Integration Team 2007], and connected with corresponding GLASS research on LoCo diagnostics. The diagnostic approaches presented here and in S09 will serve as the backbone for a broader, more rigorous analysis to include a formal evaluation of the coupling between a range of LSMs and PBLs against observations, as well as compositing and regional analysis of dry and wet regimes.

Acknowledgments. This work was supported by the NASA Energy and Water Cycle Study (NEWS; PI: C. Peters-Lidard). In particular, Jim Geiger was instrumental in providing support related to LIS–WRF coupling and testing. We also appreciate the past and ongoing collaboration with the LoCo community that has stimulated this work, in particular Michael Ek, Cor Jacobs, Obbe Tuinenburg, Bert Holtslag, Chiel van Heerwaarden, Bart van den Hurk, and Martin Best.

REFERENCES

Angevine, W. M., 1999: Entrainment results including advection and case studies from the Flatland boundary layer experiments. *J. Geophys. Res.,* **104D,** 30 947–30 963.

Barros, A. P., and W. Hwu, 2002: A study of land-atmosphere interactions during summertime rainfall using a mesoscale model. *J. Geophys. Res.,* **107D,** 4227, doi:10.1029/2000JD000254.

Betts, A. K., 1992: FIFE atmospheric boundary layer budget methods. *J. Geophys. Res.,* **97D,** 18 523–18 532.

——, 2000: Idealized model for equilibrium boundary layer over land. *J. Hydrometeor.,* **1,** 507–523.

——, 2004: Understanding hydrometeorology using global models. *Bull. Amer. Meteor. Soc.,* **85,** 1673–1688.

——, and J. H. Ball, 1994: Budget analysis of FIFE-1987 sonde data. *J. Geophys. Res.,* **99D,** 3655–3666.

——, and ——, 1995: The FIFE surface diurnal cycle climate. *J. Geophys. Res.,* **100** (D12), 25 679–25 693.

——, and P. Viterbo, 2005: Land-surface, boundary layer, and cloud-field coupling over the southwestern Amazon in ERA-40. *J. Geophys. Res.,* **110,** D14108, doi:10.1029/2004JD005702.

——, and M. A. F. Silva Dias, 2010: Progress in understanding land-surface-atmosphere coupling from LBA research. *J. Adv. Model. Earth Syst.,* **2,** doi:10.3894/JAMES.2010.2.6.

——, J. H. Ball, A. C. M. Beljaars, M. J. Miller, and P. A. Viterbo, 1996: The land surface-atmosphere interaction: A review based on observational and global modeling perspectives. *J. Geophys. Res.,* **101D,** 7209–7226.

Boone, A., and Coauthors, 2009: The AMMA Land Surface Model Intercomparison Project. *Bull. Amer. Meteor. Soc.,* **90,** 1865–1880.

Chen, F., and Y. Zhang, 2009: On the coupling strength between the land surface and the atmosphere: From viewpoint of surface exchange coefficients. *Geophys. Res. Lett.,* **36,** L10404, doi:10.1029/2009GL037980.

Cheng, W. Y. Y., and W. J. Steenburgh, 2005: Evaluation of surface sensible weather forecasts by the WRF and the Eta models over the western United States. *Wea. Forecasting,* **20,** 812–821.

Cleugh, H. A., M. R. Raupach, P. R. Briggs, and P. A. Coppin, 2004: Regional-scale heat and water vapour fluxes in an agricultural landscape: An evaluation of CBL budget methods at OASIS. *Bound.-Layer Meteor.,* **110,** 99–137.

Culf, A. D., 1994: Equilibrium evaporation beneath a growing convective boundary layer. *Bound.-Layer Meteor.,* **70,** 37–49.

Dai, Y. J., and Coauthors, 2003: The Common Land Model. *Bull. Amer. Meteor. Soc.,* **84,** 1013–1023.

De Ridder, K., 1997: Land surface processes and the potential for convective precipitation. *J. Geophys. Res.,* **102** (D25), 30 085–30 090.

Diak, G. R., 1990: Evaluation of heat flux, moisture flux and aerodynamic roughness at the land surface from knowledge of the PBL height and satellite derived skin temperatures. *Agric. For. Meteor.,* **22,** 505–508.

Dirmeyer, P. A., R. D. Koster, and Z. Guo, 2006: Do global models properly represent the feedback between land and atmosphere? *J. Hydrometeor.,* **7,** 1177–1198.

——, C. A. Schlosser, and K. L. Brubaker, 2009: Precipitation, recycling, and land memory: An integrated analysis. *J. Hydrometeor.,* **10,** 278–288.

Dolman, A., J. Gash, J. Goutorbé, Y. Kerr, T. Lebel, S. Prince, and J. Stricker, 1997: The role of the land surface in Sahelian climate: HAPEX–Sahel results and future research needs. *J. Hydrol.,* **188/189,** 1067–1079.

Ek, M. B., and A. A. M. Holtslag, 2004: Influence of soil moisture on boundary layer cloud development. *J. Hydrometeor.,* **5,** 86–99.

——, K. E. Mitchell, Y. Lin, E. Rogers, P. Grunmann, V. Koren, G. Gayno, and J. D. Tarpley, 2003: Implementation of Noah land surface model advances in the National Centers for Environmental Prediction operational mesoscale Eta model. *J. Geophys. Res.,* **108,** 8851, doi:10.1029/2002JD003296.

Eltahir, E. A., 1998: A soil moisture–rainfall feedback mechanism: 1. Theory and observations. *Water Resour. Res.,* **34,** 765–776.

Entekhabi, D., and Coauthors, 1999: An agenda for land surface hydrology research and a call for the second international hydrology decade. *Bull. Amer. Meteor. Soc.,* **80,** 2043–2058.

Ferguson, C. R., and E. Wood, 2011: Observed land–atmosphere coupling from satellite remote sensing and reanalysis. *J. Hydrometeor.,* in press.

Gu, L., and Coauthors, 2006: Direct and indirect effects of atmospheric conditions and soil moisture on surface energy partitioning revealed by a prolonged drought at a temperate forest site. *J. Geophys. Res.,* **111,** D16102, doi:10.1029/2006JD007161.

Henderson-Sellers, A., Z. L. Yang, and R. Dickinson, 1993: The Project for Intercomparison of Land-surface Parameterization Schemes. *Bull. Amer. Meteor. Soc.,* **74,** 1335–1349.

Hong, S. Y., and H. L. Pan, 1996: Nonlocal boundary layer vertical diffusion in a medium-range forecast model. *Mon. Wea. Rev.,* **124,** 2322–2339.

——, Y. Noh, and J. Dudhia, 2006: A new vertical diffusion package with an explicit treatment of entrainment processes. *Mon. Wea. Rev.,* **134,** 2318–2341.

Jacobs, C. M. J., and H. de Bruin, 1992: The sensitivity of regional transpiration to land-surface characteristics: Significance of feedback. *J. Climate,* **5,** 683–698.

——, and Coauthors, 2008: Evaluation of European Land Data Assimilation System (ELDAS) products using in situ observations. *Tellus,* **60A,** 1023–1037.

Janjic, Z. I., 2001: Nonsingular implementation of the Mellor-Yamada level 2.5 scheme in the NCEP mesoscale model. National Centers for Environmental Prediction Office Tech. Rep. 437, 61 pp.

Jarvis, P. G., and K. G. McNaughton, 1986: Stomatal control of transpiration. *Adv. Ecol. Res.,* **15,** 1–49.

Koster, R. D., and Coauthors, 2004: Regions of strong coupling between soil moisture and precipitation. *Nature,* **306,** 1138–1140.

Kumar, S. V., and Coauthors, 2006: Land Information System—An interoperable framework for high resolution land surface modeling. *Environ. Model. Software,* **21,** 1402–1415.

——, C. D. Peters-Lidard, J. L. Eastman, and W.-K. Tao, 2008: An integrated high resolution hydrometeorological modeling testbed using LIS and WRF. *Environ. Model. Software,* **23,** 169–181.

Margulis, S. A., and D. Entekhabi, 2001: Feedback between the land surface energy balance and atmospheric boundary layer diagnosed through a model and its adjoint. *J. Hydrometeor.,* **2,** 599–620.

Mellor, G. L., and T. Yamada, 1982: Development of a turbulence closure model for geophysical fluid problems. *Rev. Geophys. Space Phys.,* **20,** 851–875.

Michalakes, J., S. Chen, J. Dudhia, L. Hart, J. Klemp, J. Middlecoff, and W. Skamarock, 2001: Development of a next generation regional weather research and forecast model. *Proc. Ninth ECMWF Workshop on the Use of High Performance Computing in Meteorology,* Singapore, ECMWF, 269–276.

Monteith, J. L., and M. H. Unsworth, 1990: *Principles of Environmental Physics.* 2nd ed. Edward Arnold, 291 pp.

NASA Energy- and Water-Cycle Study (NEWS) Science Integration Team, 2007: Predicting energy and water cycle consequences of earth system variability and change. NASA Project Rep., 89 pp.

Nicholls, S. D., and K. I. Mohr, 2010: An analysis of the environments of intense convective systems in West Africa in 2003. *Mon. Wea. Rev.,* **138,** 3721–3739.

Oke, T. R., 1987: *Boundary Layer Climates.* 2nd ed. Routledge, 435 pp.

Pan, H.-L., and L. Mahrt, 1987: Interaction between soil hydrology and boundary-layer development. *Bound.-Layer Meteor.,* **38,** 185–202.

Peters-Lidard, C. D., and L. H. Davis, 2000: Regional flux estimation in a convective boundary layer using a conservation approach. *J. Hydrometeor.,* **1,** 170–182.

——, and Coauthors, 2007: High-performance Earth system modeling with NASA/GSFC's Land Information System. *Innovations Syst. Software Eng.,* **3,** 157–165.

Raupach, M. R., 2000: Equilibrium evaporation and the convective boundary layer. *Bound.-Layer Meteor.,* **96,** 107–141.

Santanello, J. A., M. A. Friedl, and W. P. Kustas, 2005: Empirical investigation of convective planetary boundary layer evolution and its relationship with the land surface. *J. Appl. Meteor.,* **44,** 917–932.

——, ——, and M. Ek, 2007: Convective planetary boundary layer interactions with the land surface at diurnal time scales: Diagnostics and feedbacks. *J. Hydrometeor.,* **8,** 1082–1097.

——, C. D. Peters-Lidard, S. V. Kumar, C. Alonge, and W.-K. Tao, 2009: A modeling and observational framework for diagnosing local land–atmosphere coupling on diurnal time scales. *J. Hydrometeor.,* **10,** 577–599.

Seneviratne, S. I., T. Corti, E. L. Davin, M. Hirschi, E. B. Jaeger, I. Lehner, B. Orlowsky, and A. J. Teuling, 2010: Investigating soil moisture–climate interactions in a changing climate: A review. *Earth Sci. Rev.,* **99,** 125–161.

Siqueira, M., G. Katul, and A. Porporato, 2009: Soil moisture feedbacks on convection triggers: The role of soil–plant hydrodynamics. *J. Hydrometeor.,* **10,** 96–112.

Sorbjan, Z., 1995: Toward evaluation of heat fluxes in the convective boundary layer. *J. Appl. Meteor.,* **34,** 1092–1098.

Steeneveld, G. J., B. J. H. van de Wiel, and A. A. M. Holtslag, 2006: Modeling the evolution of the atmospheric boundary layer coupled to the land surface for three contrasting nights in CASES-99. *J. Atmos. Sci.,* **63,** 920–935.

Troen, I., and L. Mahrt, 1986: A simple model of the atmospheric boundary layer: Sensitivity to surface evaporation. *Bound.-Layer Meteor.,* **37,** 129–148.

Van den Hurk, B. J. J. M., and E. M. Blyth, 2008: WATCH/LoCo workshop report. *GEWEX News,* Vol. 18, No. 4, International GEWEX Project Office, Silver Spring, MD, 12–14.

Van Heerwaarden, C. C., J. Vilà-Guerau de Arellano, A. F. Moene, and A. A. M. Holtslag, 2009: Interactions between dry-air entrainment, surface evaporation and convective boundary-layer development. *Quart. J. Roy. Meteor. Soc.,* **135,** 1277–1291.

Weckworth, T. M., and Coauthors, 2004: An overview of the International H_2O Project (IHOP_2002) and some preliminary highlights. *Bull. Amer. Meteor. Soc.,* **85,** 253–277.

Zhang, Y., and S. A. Klein, 2010: Mechanisms affecting the transition from shallow to deep convection over land: Inferences from observations of the diurnal cycle collected at the ARM Southern Great Plains site. *J. Atmos. Sci.,* **67,** 2943–2959.